Available online at www.sciencedirect.com
ScienceDirect
Journal of Photochemistry and Photobiology A: Chemistry 193 (2008) 153–160
Journal of Photochemistry and Photobiology A:Chemistry
www.elsevier.com/locate/jphotochem

# Performance of near-IR luminescent xerogel materials covalently bonded with ternary lanthanide ($Er^{III}$, $Nd^{III}$, $Yb^{III}$) complexes

Li-Ning Sun [a,b], Hong-Jie Zhang [a,*], Jiang-Bo Yu [a], Qing-Guo Meng [a], Feng-Yi Liu [a], Chun-Yun Peng [a]

[a] *Key Laboratory of Rare Earth Chemistry and Physics, Changchun Institute of Applied Chemistry, Chinese Academy of Sciences, Changchun 130022, PR China*
[b] *Graduate School of the Chinese Academy of Sciences, Beijing, PR China*

Received 13 March 2007; received in revised form 18 May 2007; accepted 15 June 2007
Available online 20 June 2007

**Abstract**

A series of near-infrared (NIR) luminescent ternary lanthanide (Ln = Er, Nd, Yb) complexes covalently linked to xerogels by a chelate ligand 5-(*N*,*N*-bis-3-(triethoxysilyl)propyl)ureyl-1,10-phenanthroline (phen-Si) were synthesized in situ via a sol–gel method. The obtained xerogel materials (named xerogel-bonded Ln complex) are rigid, and appear homogeneous confirmed by SEM images. Upon excitation at the maximum absorption wavelength of the ligands, all these xerogel materials with different lanthanide complex concentration show the characteristic NIR luminescence of the corresponding lanthanide ion, as a result of the efficient energy transfer from the ligands to the lanthanide ion. For the xerogel-bonded Er complex, the full width at half maximum (FWHM) of the $^4I_{13/2} \rightarrow {}^4I_{15/2}$ transition is 76 nm, which enables a wide gain bandwidth for the optical amplification. Based on the Judd–Ofelt theory, the radiative properties of the xerogel-bonded Nd complex (with Nd/Si molar ratio of 1/11 in the reaction) were studied.


*Keywords:* NIR luminescence; Covalently bonded; Ternary lanthanide complex; Xerogel material; Judd–Ofelt theory

## 1. Introduction

Recently, much attention has been paid to near-infrared (NIR) luminescence of trivalent lanthanide complexes, such as Yb(III), Er(III) and Nd(III), due to their potential applications from biomolecule labeling in luminescent bioassays (based on Yb complexes) [1,2] to functional materials for optical telecommunication network (based on Er complexes) [3–5] and laser systems (based on Nd complexes) [6–8]. For practical applications, it is advantageous to embed these NIR luminescent complexes in a stable rigid matrix. Sol–gel derived hybrid materials have attracted much interest for photonic applications, as they potentially combine the optical quality of silica, its thermal stability and mechanical strength, together with the optical characteristics of active organic molecules [9–12]. The obvious advantages of the sol–gel method include the mild reaction conditions, the feasibility to control the composition easily and the convenient preparation routes [13–16]. Therefore, sol–gel hybrid materials are potential hosts for NIR-luminescent lanthanide complexes. In the recent years, more effort has been devoted to covalent grafting of the ligands to the backbone of sol–gel via Si–C bonds, because the solubility and homogeneous distribution of lanthanide complexes in the material can be improved by covalently linking the complexes to the matrix [17–21]. Recently, our group has reported the synthesis of functionalized 1,10-phenanthroline ligand 5-(*N*,*N*-bis-3-(triethoxysilyl)propyl)ureyl-1,10-phenanthroline (phen-Si), through which the binary europium phenanthroline complex was covalently attached to the silica-based network [22]. And Binnemans et al. reported the covalent grafting of some ternary lanthanide complexes to the sol–gel via the phen-Si ligand by a ligand exchange reaction [23,24]. Yet, in the previous reports the optical properties of the luminescent sol–gel materials have not been studied in detail.

In the present paper, the NIR-luminescent xerogel materials covalently bonded with lanthanide complex via the recently developed in situ approach [13–15] were synthesized and the

* Corresponding author. Tel.: +86 431 85262127; fax: +86 431 85698041.
*E-mail address:* hongjie@ns.ciac.jl.cn (H.-J. Zhang).

1010-6030/$ – see front matter © 2007 Elsevier B.V. All rights reserved.
doi:10.1016/j.jphotochem.2007.06.020

luminescent properties of the materials have been demonstrated in detail. The NIR-luminescent materials (denoted xerogel-bonded Ln complex(*N*), where *N* is the Ln/Si molar ratio in the reaction) consist of ternary lanthanide complexes [$Ln(dbm)_3phen$; Ln = Er, Nd, Yb; dbm = dibenzoylmethanate] covalently bonded to the sol–gel matrix by the phen-Si ligand. No cracks were observed in the obtained xerogels. And the xerogel materials were very rigid. The NIR-luminescence behavior of these materials with different lanthanide complex concentrations has been studied. Based on the Judd–Ofelt theory and the experimental absorption spectrum, the optical properties of the xerogel-bonded Nd complex(1/11) have been investigated.

## 2. Experimental

### 2.1. Materials

Tetraethoxysilane (TEOS, Aldrich), 3-(triethoxysilyl)-propyl isocyanate (Aldrich), fuming nitric acid and absolute ethanol were used as received. The solvent chloroform ($CHCl_3$) was used after desiccation with anhydrous calcium chloride. Ytterbium oxide ($Yb_2O_3$, 99.99%), neodymium oxide ($Nd_2O_3$, 99.99%) and erbium oxide ($Er_2O_3$, 99.99%) were purchased from Yue Long Chemical Plant (Shanghai, China). 1,10-Phenanthroline monohydrate (Phen·$H_2O$, 99%, A.R.), and dibenzoylmethane (Hdbm, C.P.) were bought from Beijing Fine Chemical Co. (Beijing, China). $LnCl_3$ (Ln = Er, Nd, Yb) was obtained by dissolving $Ln_2O_3$ in hydrochloric acid.

### 2.2. Synthesis of the xerogel-bonded ln complex (Ln = Er, Nd, Yb)

The starting reagent 5-amino-1,10-phenanthroline (denoted as phen-$NH_2$) was prepared according to the procedure described in the literature [25]. The modified phenanthroline (phen-Si) was synthesized by the reaction of phen-$NH_2$ and 3-(triethoxysilyl)-propyl isocyanate in $CHCl_3$ as described in ref. [21]. Analysis: calculated for $C_{32}H_{51}N_5O_8Si_2$: C, 55.5; H, 7.4; N, 10.0%. Found: C, 55.0; H, 7.1; N, 10.9%. NMR ($CDCl_3$), $\delta$ 0.520 (4H, m); 1.133 (18H, t); 1.606 (4H, m); 3.223 (4H, q); 3.687 (12H, q); 7.270 (2H, brs); 7.680 (2H, m); 7.855 (1H, s), 8.238 (2H, m); 9.225 (2H, m).

Phen-Si was dissolved in ethanol, and then TEOS and deionized water (acidified with HCl, pH = 2) were added under stirring. An appropriate amount of Hdbm and $LnCl_3$ ethanol solution were introduced into the starting solution consecutively. The molar ratio of phen-Si:TEOS:$H_2O$:$Ln^{3+}$:Hdbm was 1:*x*:4*x*:1:3 (*x* = 25 and 9). The mixed solution was stirred for about 4 h at room temperature to ensure homogeneous mixing and achieve a single phase, and then placed in a cuvette. The precursor solution converted to wet gel after several days of gelation at 45 °C and then was continuously dried to obtain a transparent monolithic xerogel. The lanthanide complexes were supposed to be in situ synthesized during the corresponding sol-to-xerogel conversion accompanied with the evaporation of HCl, respectively. Monolithic xerogel samples were ground for the luminescence and SEM measurements. The obtained powder materials were washed with acetone and ethanol for removal of the surplus $Ln^{3+}$ ion and Hdbm, and all of the complexes in the materials were attached to the matrix by the functionalized phen groups. The obtained materials were denoted as xerogel-bonded Ln complex(*N*), where *N* is the Ln/Si molar ratio in the initial mixture, and it is 1/27 and 1/11 when *x* equals 25 and 9, respectively. Before the luminescence measurements were made, the materials were powdered again and dried under vacuum for 24 h at 80 °C.

### 2.3. Characterization

All measurements were carried out at room temperature. Scanning electron micrographs were obtained using a JSM-6700F microscope operating at 10.0 kV. FT-IR spectra were measured within a 4000–400 $cm^{-1}$ region on an American Bio-Rad Company model FTS135 infrared spectrophotometer with the KBr pellet technique. The fluorescence spectra were recorded on an Edinburgh Analytical Instruments FLS920 equipped with a stablespec-Xenon lamp (450 W) as the light source with the samples in solid state as powder. The time-resolved measurements, for xerogel-bonded Yb complex(1/11) was made on the same instrument (monitored at 980 nm), for xerogel-bonded Er complex(1/11) was done on an Edinburgh Instruments Combined Luminescence Lifetime and Steady State Spectrometer FLS920 equipped with a μF900 Lamp (monitored at 1535 nm), and for xerogel-bonded Nd complex(1/11) was done by using the third harmonic (355 nm) of a Spectra-physics Nd:YAG laser with a 5 ns pulse width and 5 mJ of energy per pulse as the source, an emission monochromator (Acton 2758) equipped with a Hamamatsu R5108 photomultiplier tube and the data were analysed with a LeCroy WaveRunner 6100 1 GHz Oscilloscope (monitored at 880 nm). The xerogel sample, 5.30 mm in diameter and 5.26 mm in thickness, was applied to the optical absorption measurement. The spectral optical density $OD(\lambda) = 0.4343 l\rho\sigma(\lambda)$ of the xerogel-bonded Nd complex(1/11) was recorded using a Shimadzu UV-3101 PC at room temperature, where $l$ is the thickness of the xerogel, $\sigma(\lambda)$ the absorption cross-section and $\rho$ is the concentration of $Nd^{3+}$ ion in the xerogel. The corresponding concentration is calculated to be $3.0 \times 10^{20}$ Nd/$cm^3$, using the expression $\rho = (nN)/(\pi(R/2)^2 l)$, where $n$ is the molar number of $Nd^{3+}$ ion, $N$ is $6.02 \times 10^{23}$ and $R$ is the diameter.

## 3. Results and discussion

Because of the presence of numerous hydroxyl groups (in Si–OH and $H_2O$) that act as nonradiative channels for the excited states of the lanthanide ions, the observation of NIR luminescence by lanthanide ions in silica sol–gel material is not common compared with that of the visible luminescence by Eu(III) and Tb(III), etc. The concentration of hydroxyl groups is high in gels and has strong quenching properties toward the luminescence of lanthanide complexes. The most common method to decrease the degree of quenching is to calcine the sol–gel materials at high temperature (>900 °C). However, the sensitizer ligands usually decompose at such high calcination tempera-

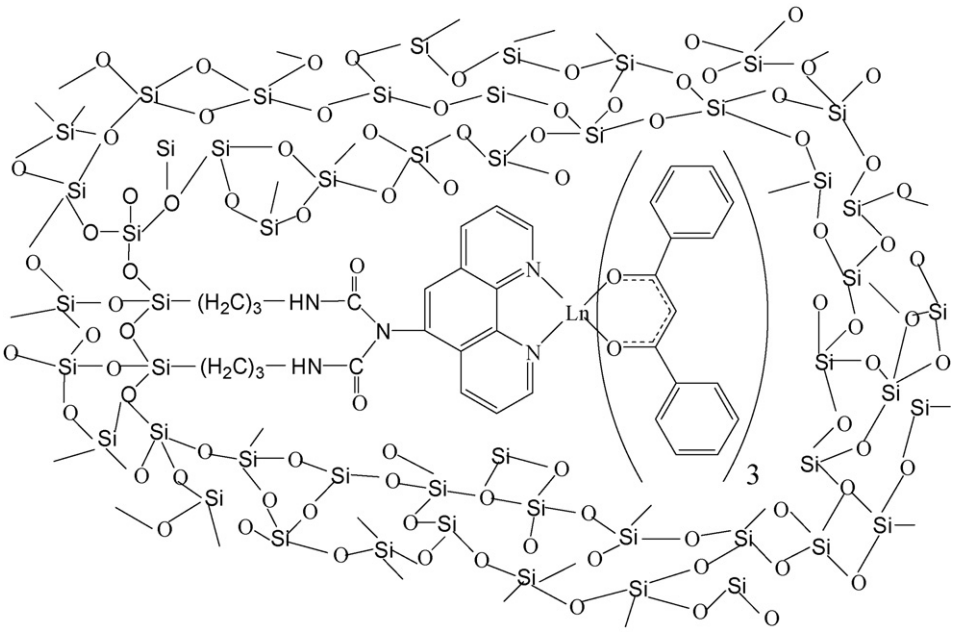


Scheme 1. Proposed structure of the xerogel-bonded Ln complex(*N*), Ln = Er, Nd, Yb.

ture. In our case, the co-condensation of TEOS and phen-Si, where some –OH groups are substituted by organic groups and hence the increased hydrophobicity of the modified materials is achieved, might effectively depress the nonradiative multiphonon relaxation through –OH groups. Therefore, the phen-Si plays a triplex role during the sol–gel process, i.e. as a precursor for the sol–gel, as a ligand for the lanthanide ions, and as a silylation agent for the precursor in the sol–gel process. During the co-condensation of TEOS and phen-Si, the $Ln^{3+}$ ion and the other ligand Hdbm were introduced, and thus all the compositions were mixed at a molecular level. In this way, the lanthanide complex was supposed to be in situ synthesized and coupled to the silica backbone during the corresponding sol-to-xerogel conversion accompanied with the evaporation of HCl [16]. All the xerogels prepared are very transparent and rigid. The expected structure of the xerogel material formed is shown in Scheme 1.

All the xerogel-bonded Ln complex(*N*) (Ln = Er, Nd and Yb) exhibit very similar FT-IR spectra, as illustrated by the representative pattern of xerogel-bonded Er complex(1/11). Fig. 1 shows the FT-IR spectra of phen-Si and xerogel-bonded Er complex(1/11). In Fig. 1a, the spectrum of phen-Si is dominated by $\nu$(C–Si, 1193 $cm^{-1}$) and $\nu$(Si–O, 1079 $cm^{-1}$) absorption bands which are characteristic of trialkoxylsilyl functions. The introduction of TEOS, the $Ln^{3+}$ ion, and the ligand Hdbm to Phen-Si is responsible for some changes in the IR spectrum of xerogel-bonded Er complex(1/11) as shown in Fig. 1b. This is due to the hydrolysis/condensation of TEOS and Phen-Si and the formation of complex between $Ln^{3+}$ ion and ligands phen-Si and dbm. In Fig. 1b, the peak at 1080 $cm^{-1}$ can be attributed to Si–O symmetric stretching vibration and the band at 450 $cm^{-1}$ corresponds to the bending vibration of Si–O–Si band, which indicates the formation of the Si–O–Si framework. The bands at 1651 and 1528 $cm^{-1}$, originating from the CONH group of phen-Si, can also be observed in Fig. 1b, which is consistent with the fact that the functionalized phen group in the framework remains intact.

The scanning electron micrographs of the xerogel-bonded Ln complex(*N*) (Ln = Er, Nd and Yb) are similar, as displayed by the representative patterns of xerogel-bonded Er complex(1/11). From the SEM in Fig. 2, it is shown that the material appears homogeneous, and no sign of any phase separation was observed even when the magnification was increased to 30,000. There are two possible factors to explain the phenomenon. One possibility is the in situ synthesis technique we used, through which all the compositions are mixed at a molecular level [13–15], another is the strong covalent bonds bridging between the inorganic and organic phases [26]. As a result, the material is composed quite uniformly and is one-component hybrid organic–inorganic material, so that the inorganic and organic phases might exhibit their distinct properties together [19,20].

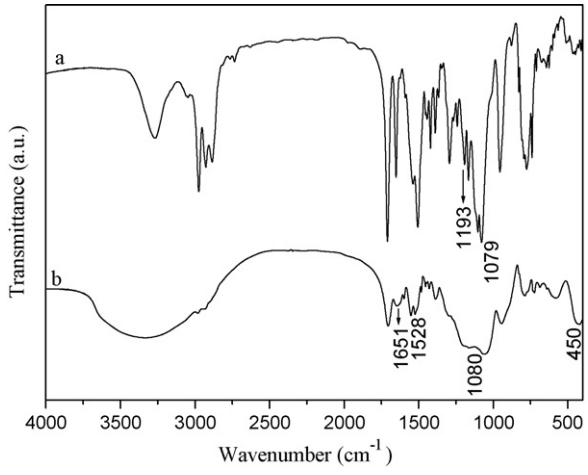


Fig. 1. FT-IR spectra of (a) phen-Si and (b) xerogel-bonded Er complex(1/11).

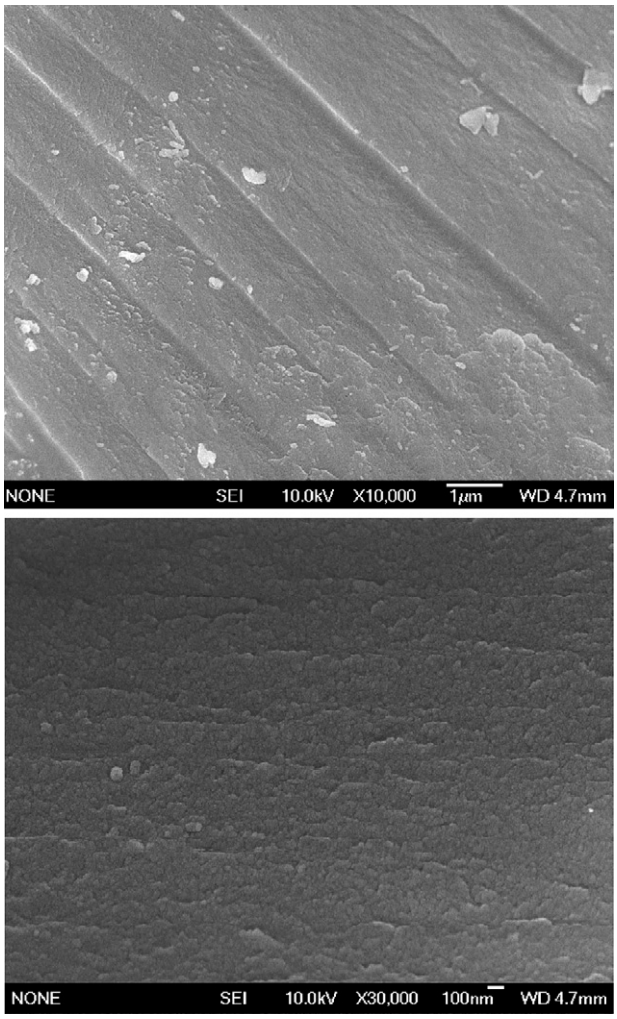


Fig. 2. Scanning electron micrograph images of xerogel-bonded Er complex(1/11).

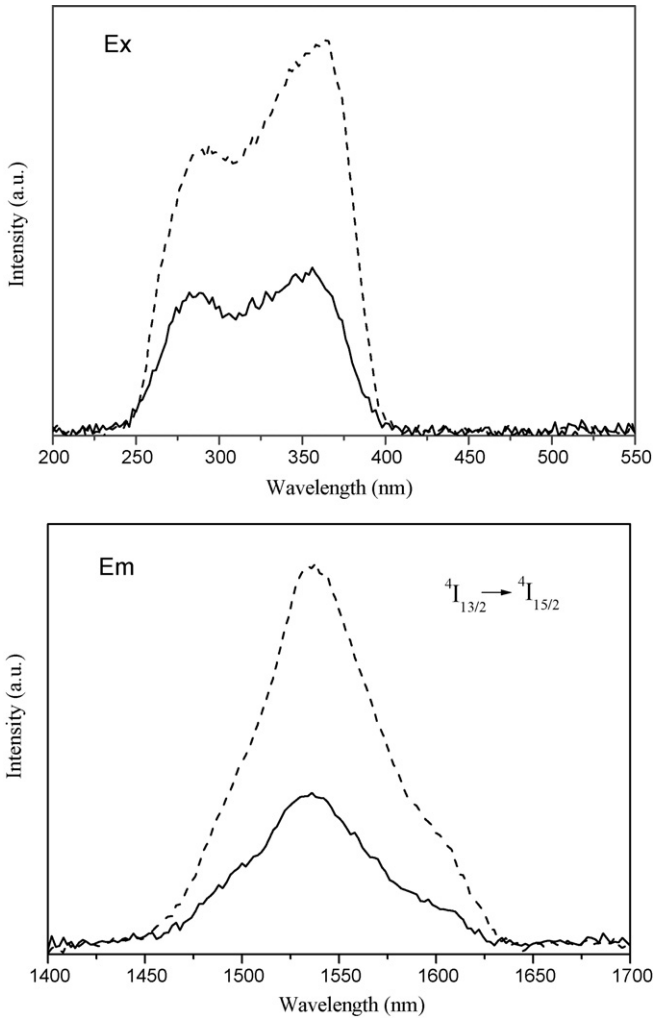


Fig. 3. Excitation ($\lambda_{em}$ = 1541 nm) and emission ($\lambda_{ex}$ = 365 nm) spectra for xerogel-bonded Er complex(1/11) (dashed line) and xerogel-bonded Er complex(1/27) (solid line).

Fig. 3 presents the excitation and emission spectra of xerogel-bonded Er complex(*N*) (*N* = 1/27 and 1/11) materials. The two excitation spectra monitored at 1535 nm are composed of a broad band in the ultraviolet/visible spectral range, which is due to the light absorption by the dbm and functionalized phen ligands. Compared with the pure $Er(dbm)_3phen$ complex [16], the xerogel-bonded Er complex(*N*) show the narrower ligands absorption band, and the maximum excitation wavelengths shift from 415 to 365 and 356 nm for xerogel-bonded Er complex(*N*), *N* = 1/11 and 1/27, respectively. This is probably because that the complex molecules are dispersed and further confined strictly by the rigid silica network after being incorporated into the silica matrix. Due to the "cage effect", some vibrations of ligands are weakened. Therefore, the absorption band of the ligands in the xerogel-bonded Er complex(*N*) becomes narrower [27]. In addition, in the excitation spectrum of pure $Er(dbm)_3phen$ complex some small peaks, originating from f to f absorption transitions of $Er^{3+}$ ion, are observed [16], yet no f–f transition of $Er^{3+}$ ion could be observed in those of the xerogel-bonded Er complex(*N*) (*N* = 1/27 and 1/11), respectively. This suggests that the energy transfer from the ligands to the $Er^{3+}$ ion is more efficient in the xerogel-bonded Er complex(*N*) than that in the pure $Er(dbm)_3phen$ complex, i.e. an improvement of $Er^{3+}$ ion sensitized process [28]. Another possible explanation is due to the lower $Er^{3+}$ ion content in the xerogel-bonded Er complex(*N*). After ligand-mediated excitation at 365 nm, both the emission spectra of the xerogel-bonded Er complex(*N*) (*N* = 1/27 and 1/11) clearly show the emission bands centered at 1535 nm, respectively, which are attributed to the transition from the first excited state ($^4I_{13/2}$) to the ground state ($^4I_{15/2}$) of the $Er^{3+}$ ion. Recently, erbium-doped materials have attracted considerable attention in optical amplification because the transition around 1540 nm is just at the position for the telecom applications (erbium-doped fiber amplifiers). To enable a wide gain bandwidth for optical amplification, a broad emission band is desirable [29]. The full widths at half maximum (FWHM) of the $^4I_{13/2} \rightarrow {}^4I_{15/2}$ transition for the xerogel-bonded Er complex(*N*) (*N* = 1/27 and 1/11) both are 76 nm and are wider than that of the sol–gel material doped with the erbium complex (72 nm), in which only physical interactions exist between the silica matrix and the complex [16]. Such wide bandwidth indicates that $Er^{3+}$

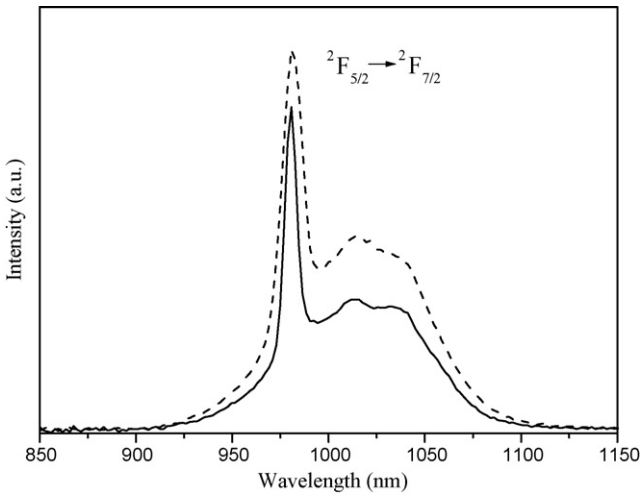


Fig. 4. Emission ($\lambda_{ex}$ = 365 nm) spectra for xerogel-bonded Yb complex(1/11) (dashed line) and xerogel-bonded Yb complex(1/27) (solid line).

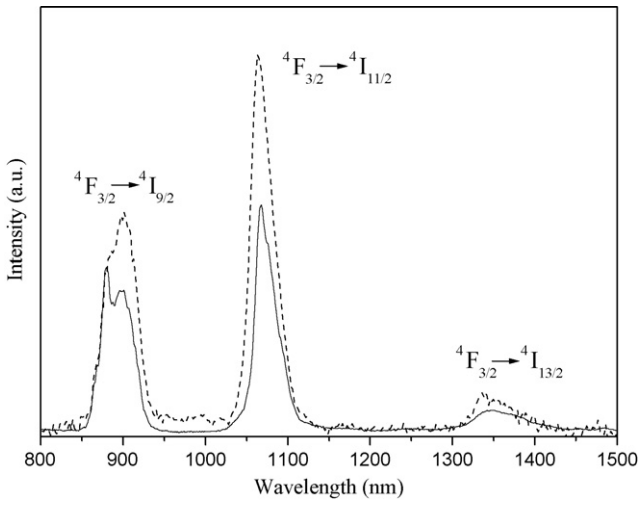


Fig. 5. Emission ($\lambda_{ex}$ = 365 nm) spectra for xerogel-bonded Nd complex(1/11) (dashed line) and xerogel-bonded Nd complex(1/27) (solid line).

ions have different local environments in the xerogels, which enables a wide gain bandwidth for optical amplification [30].

The excitation spectra of xerogel-bonded Ln (Nd, Yb) complex(*N*) (*N* = 1/27 and 1/11) are similar to those of xerogel-bonded Er complex(*N*) (*N* = 1/27 and 1/11), respectively, and also show broad bands due to the absorption of the organic ligands. Upon excitation of the ligands absorption bands at 365 nm, the emission spectra (Fig. 4) of xerogel-bonded Yb complex(*N*) (*N* = 1/27 and 1/11) were obtained, respectively. In both curves, the prominent 980 nm emission band can be observed, which is assigned to the $^2F_{5/2} \rightarrow {}^2F_{7/2}$ transition of the $Yb^{3+}$ ion. In comparison with other lanthanide-centered emission peaks, the Yb(III) emission is broad. This is due to the vibronic coupling between the electronic state of Yb and the vibrational states of the ligand. It should also be noted that the $Yb^{3+}$ ion emission band is not a single sharp band but an envelope of bands arising at lower energy side than the primary 980 nm band. Similar splitting has been reported previously, and this may be due to the splitting of the energy levels of the $Yb^{3+}$ ion as a consequence of ligand field effects [31,32]. The $Yb^{3+}$ ion has some advantages for laser emission because of its very simple f–f energy level structure: besides the $^2F_{7/2}$ ground state, there is only the $^2F_{5/2}$ excited state. The smaller Stokes shift (around 650 $cm^{-1}$) between absorption and emission reduces the thermal loading of the material during laser operation [33]. In addition, the relative transparency of human tissue at approximately 1000 nm suggests that in vivo luminescent probes operating at this wavelength (based on Yb emission of the xerogels) might have diagnostic value [34].

The emission spectra (Fig. 5) of xerogel-bonded Nd complex(*N*) (*N* = 1/27 and 1/11) were obtained with 365 nm as the excitation wavelength. In the two spectra, both the curves consist of three bands, at 901, 1063 and 1336 nm for xerogel-bonded Nd complex(1/11) and at 880, 1067 and 1346 nm for xerogel-bonded Nd complex(1/27), which correspond to the $^4F_{3/2}$ (emitting level) $\rightarrow {}^4I_{9/2}$, $^4F_{3/2} \rightarrow {}^4I_{11/2}$ and $^4F_{3/2} \rightarrow {}^4I_{13/2}$ transitions, respectively. Among the three bands of the emission spectra, the intensity of the transition $^4F_{3/2} \rightarrow {}^4I_{11/2}$ is the strongest, and this center has been found potential application in laser systems for long.

As described above, the characteristic $Ln^{3+}$ ion emission was detected in the corresponding xerogel-bonded Ln complex(*N*) (*N* = 1/27 and 1/11) upon excitation at the absorption of the organic ligands. It is obvious that the intramolecular energy transfer does happen between the organic ligands and the lanthanide ion. And it is reasonable to deduce that the lanthanide complex was synthesized in the corresponding xerogel-bonded Ln complex(*N*). It is also noted that the relative emission intensity of the xerogel-bonded Ln complex(*N*) (Ln = Er, Nd, Yb) increases when increasing the lanthanide complex concentration. Then we can infer, in a qualitatively way, that no quenching effects were detected with increasing concentration from *N* = 1/27 to 1/11, as the experimental conditions (such as excitation power and detection slits) were kept constant during the entire set of measurements. Time-resolved measurements were carried out on the xerogel-bonded Ln complex(1/11) at room temperature. The luminescence decays for these materials are single-exponential functions of time, and the corresponding lifetimes of the Er($^4I_{13/2}$), Nd($^4F_{3/2}$) and Yb($^2F_{5/2}$) levels are 1.04 μs, 443 ns and 15.03 μs, respectively.

The Judd–Ofelt theory is widely used and remarkably successful for quantitatively characterizing optical 4f transitions in lanthanide-doped materials [35,36]. As discussed above, the xerogel-bonded Nd complex(1/11) with high intensity emission has the possibility to be used in the laser systems. To further evaluate the potential of lanthanide-doped materials, it is essential to study the radiative properties of the lanthanide ion. As usual, the radiative properties of the trivalent lanthanide ion in the host can be predicted from optical absorption measurement and by using the Judd–Ofelt theory. As for the details of the Judd–Ofelt theory, its accuracy and drawbacks have been extensively analyzed elsewhere; we present here only the essential results [35–38].

As discussed for parity-forbidden electric-dipole transitions of lanthanide ion in Judd–Ofelt theory [35,36], the energy states of the $Nd^{3+}$ ion should be effectively perturbed by the odd terms

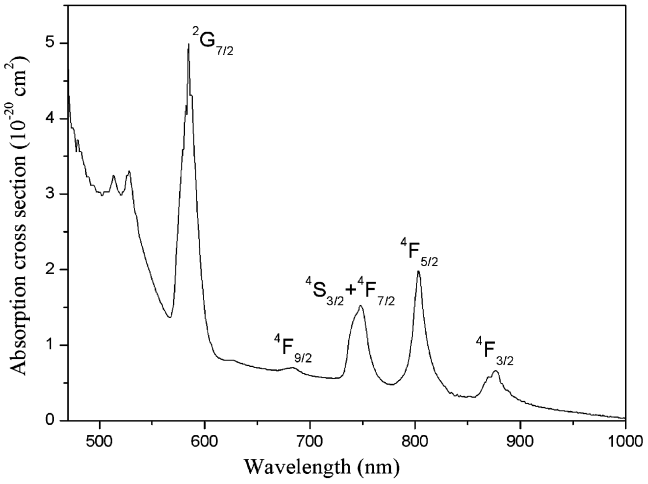


Fig. 6. Absorption spectrum of the xerogel-bonded Nd complex(1/11).

of the Hamiltonian of the weak crystal field. Although the 4f electrons are partially screened by the $5s^2$ and $5p^6$ electron shells, the perturbations can still cause the permitted transitions of the 4f electrons between the 4f energy levels [39]. As shown in Fig. 6, all the absorption peaks can be assigned to the transitions from the ground level $^4I_{9/2}$ to the higher levels of $Nd^{3+}$ ion. Five absorption bands of the $Nd^{3+}$ ion in the absorption spectrum were selected to determine the phenomenological oscillator strength parameters. The band positions along with their assignments in the absorption spectrum are shown in Table 1. The measured line strength, $S_{mea}(J \rightarrow J')$, caused by the transition of electronic dipole can be related to the absorption coefficient as the following equation shows [40,41]

$$S_{mea}(J \rightarrow J') = \frac{3ch(2J+1)n}{8\pi^3 \bar{\lambda} e^2} \left[\frac{9}{(n^2+2)^2}\right] \Gamma \quad (1)$$

where $J$ (for $Nd^{3+}$ ion $J = 9/2$) and $J'$ are the total angular momentum quantum numbers of the initial and final states, respectively, and $\bar{\lambda}$ is the mean wavelength of the specific absorption band. $e$, $h$ and $c$ are the electron charge, the Plancks' constant and velocity of light, respectively. $\Gamma = \int \sigma(\lambda)\, d\lambda$ is the integrated absorption coefficient as a function of $\lambda$. An average index of refraction of 1.5 was used [42,43], and the factor $[9/(n^2+2)^2]$ in the equation represents the local field correction for electric dipole transition for the effective field for the ion in the dielectric host medium of isotropic refractive index $n$ [44].

Table 1
Measured and calculated line strengths of $Nd^{3+}$ ion in xerogel-bonded Nd complex(1/11) (all transitions are from $^4I_{9/2}$ state)

| Level | λ (nm) | $S_{mea}$ ($\times 10^{-20}$ cm$^2$) | $S_{cal}$ ($\times 10^{-20}$ cm$^2$) |
|---|---|---|---|
| $^2G_{7/2}$ | 585 | 7.9677 | 7.9678 |
| $^4F_{9/2}$ | 684 | 0.1383 | 0.2376 |
| $^4S_{3/2}$ | 748 | 2.0056 | 2.1232 |
| $^4F_{7/2}$ | | | |
| $^4F_{5/2}$ | 803 | 2.3438 | 2.1077 |
| $^4F_{3/2}$ | 877 | 0.8027 | 1.0194 |

The measured line strengths are used to obtain the phenomenological parameters $\Omega_2$, $\Omega_4$ and $\Omega_6$ by solving a set of five equations simultaneously for the corresponding transitions between $J$ and $J'$ manifolds in the following form:

$$S_{cal}(J \rightarrow J') = \sum_{t=2,4,6} \Omega_t \left| \left\langle (S, L)J || U^{(t)} || (S', L')J' \right\rangle \right|^2 \quad (2)$$

where $\Omega_2$, $\Omega_4$ and $\Omega_6$ are the oscillator strength parameters and $\langle || U^{(t)} || \rangle$ are the doubly reduced matrix elements of rank $t$ ($t = 2$, 4 and 6) between states characterized by the quantum numbers ($S$, $L$ and $J$) and ($S'$, $L'$ and $J'$). The matrix elements depend only on angular momentum of the $Nd^{3+}$ ion states and are essentially independent of the ion environment [45]. The squared reduced matrix elements can be calculated. In this work, we have used these values for the chosen $Nd^{3+}$ bands calculated by Carnall et al. [46]. When two or more absorption manifolds overlapped, the matrix element was taken to be the sum of the corresponding squared matrix elements [47]. The oscillator strength parameters, however, exhibit the influence of the host on the transition probabilities since they contain the crystal-field parameters, the interconfigurational radial integrals, and the interaction between the central ion and the intermediate environment [44]. They may be regarded as phenomenological parameters that characterize the radiative transition probabilities within the ground configuration. The values of the measured line strength, $S_{mea}$, are shown in Table 1. Then the parameters $\Omega_t$ can be obtained by least-squares fitting of Eq. (2). We used the least-square fit in this study because almost all the $\Omega_t$ sets reported in the literature have been determined by this method. The parameters $\Omega_t$ ($t = 2$, 4 and 6) in this work have been fitted to be $94.88 \times 10^{-20}$, $3.771 \times 10^{-20}$ and $2.818 \times 10^{-20}$ cm$^2$, respectively.

The interpretation of the physical meaning of the oscillator strength parameters still remains to be a controversial matter for discussion. The $\Omega_2$-parameter is associated with short-range coordination effects, and its value increases with increasing coordination number and higher covalence of the bonding [48]. In the sense of the dynamic coupling contribution to the total intensity, the polarization of the ligand field induces stronger lanthanide–ligand bonds and an increase in electric dipolar transitions for noncentrosymmetric ligand fields [49]. It is suggested that upon covalently bonded to the xerogel, the $\Omega_2$-parameter of the xerogel-bonded Nd complex(1/11) increased when compared with the material doped of the Nd complex [50]. The larger value for $\Omega_2$ in this work suggests that the dbm and phen-Si ligands bind more strongly with the $Nd^{3+}$ ion and shield the $Nd^{3+}$ ion from the water molecules [48,51]. In addition, Jørgensen and Reisfeld concluded that the $\Omega_6$-parameter is related to the rigidity of the medium in which the lanthanide ion is embedded. More rigid matrices have lower $\Omega_6$ values [51]. In this work, as the Nd complex is covalently linked to the xerogel, the $\Omega_6$ value decreases when compared with that of the material doped of the Nd complex. This suggests that the more rigid material was obtained in our work, as it is the case.

The values of the parameters are then used to recalculate the transition line strengths $S_{cal}$ of the electric-dipole transition

Table 2
The spectral parameters for $^4F_{3/2} \rightarrow {}^4I_J$ transition of $Nd^{3+}$ ion in xerogel-bonded Nd complex(1/11)

| $^4F_{3/2} \rightarrow (\bar{S}, \bar{L})\bar{J}$ | $\lambda_p$ (nm) | $S_{cal}$ ($\times 10^{-20}$ cm$^2$) | $A$ (s$^{-1}$) | $\beta$ | $\sigma_p$ ($\times 10^{-20}$ cm$^2$) |
|---|---|---|---|---|---|
| $^4F_{3/2} \rightarrow {}^4I_{9/2}$ | 901.4 | 1.0191 | 780.6 | 0.481 | 0.413 |
| $^4F_{3/2} \rightarrow {}^4I_{11/2}$ | 1063.2 | 1.5849 | 708.3 | 0.437 | 1.161 |
| $^4F_{3/2} \rightarrow {}^4I_{13/2}$ | 1336.2 | 0.5876 | 132.6 | 0.082 | 0.325 |
| $\tau_r$ (μs) | | 616 | | | |

between the initial $J$ manifold $|(S,L)J\rangle$ and the final $J'$ manifold $|(S',L')J'\rangle$ by using Eq. (2). The calculated line strengths $S_{cal}$ of the five absorption bands are tabulated in Table 1. To justify the results obtained, a measure of the accuracy of the fit is given by the root-mean-square (rms) deviation of the measured and calculated line strengths, which is obtained by

$$\Delta S_{rms} = \left[(P - N_{para})^{-1} \sum (S_{mea} - S_{cal})^2\right]^{1/2}, \quad (3)$$

where $(S_{mea} - S_{cal})$ is the deviation, $P$ the number of spectral bands analyzed and $N_{para}$ is the number of parameters determined. In this case $N_{para}$ is three. The values in Table 1 provide an rms deviation of $0.251 \times 10^{-20}$ cm$^2$.

Using the obtained $\Omega_t$-parameters, the radiative decay rates, $A(J' \rightarrow \bar{J})$, for electric dipole transitions between an excited $J'$ state $|(S',L')J'\rangle$ and the lower-lying terminal $\bar{J}$ manifolds $\left|(\bar{S}, \bar{L})\ \bar{J}\right\rangle$ can be obtained using the following expression:

$$A[(S', L')J'; (\bar{S}, \bar{L})\bar{J}] = \frac{64\pi^4 e^2}{3h(2J'+1)\bar{\lambda}^3} \frac{n(n^2+2)^2}{9} \times \sum_{t=2,4,6} \Omega_t \left|\left\langle (S', L')J' \left\| U^{(t)} \right\| (\bar{S}, \bar{L})\bar{J} \right\rangle\right|^2 \quad (4)$$

where $(S',L')J'$ and $(\bar{S}, \bar{L})\bar{J}$ are the quantum numbers of the excited state and lower states, respectively, $J' = 3/2$ and $\bar{\lambda}$ is the mean wavelength of the emission transition (Fig. 5). The related reduced matrix elements of the emissive transitions are cited from the ref for $Nd^{3+}$ ion [52]. In fact, $Nd^{3+}$ ion has an emission band at 1900 nm ($^4F_{3/2} \rightarrow {}^4I_{15/2}$) except the obtained three emission bands. Our setup did not allow us to record the 1900 nm emission band, but it is known on the basis of Judd–Ofelt theory that this transition is exceedingly weak and can therefore be safely neglected [53].

The radiative lifetime of an emitting state is related to the total spontaneous emission probability for all transitions from this state by [54]

$$\tau_r = \frac{1}{\sum_{\bar{S},\bar{L},\bar{J}} A[^4F_{3/2}; (\bar{S}, \bar{L})\bar{J}]} \quad (5)$$

The fluorescence branching ratio of transitions from initial manifold $^4F_{3/2}$ to lower levels $\left|(\bar{S}, \bar{L})\ \bar{J}\right\rangle$ is given by

$$\beta[^4F_{3/2}; (\bar{S}, \bar{L})\bar{J}] = \frac{A[^4F_{3/2}; (\bar{S}, \bar{L})\bar{J}]}{\sum_{\bar{S},\bar{L},\bar{J}} A[^4F_{3/2}; (\bar{S}, \bar{L})\bar{J}]} = A[^4F_{3/2}; (\bar{S}, \bar{L})\bar{J}]\tau_r. \quad (6)$$

The fluorescence branching ratio is a critical parameter to the laser designer, because it characterizes the possibility of attaining stimulated emission from any specific transition [38]. The radiative lifetime represents an effective average over site-to-site variations in the local $Nd^{3+}$ ion environment and it has been calculated to be 616 μs, which is an important parameter in consideration of the pumping requirement for the threshold of laser action [55]. The estimated quantum yield of Nd luminescence of the xerogel-bonded Nd complex(1/11) may be calculated by comparison of the observed luminescence lifetime ($\tau$) with the radiative lifetime ($\tau_r$). By using the equation $\Phi = \tau/\tau_r$, the value of quantum yield is calculated to be 0.072%.

With the corresponding emission spectrum, for a Lorentz line, the stimulated emission cross-section $\sigma_p$ can be related to the radiative transition rate by

$$\sigma_p = \frac{{\lambda_p}^2}{4\pi^2 n^2\, \Delta\nu} A \quad (7)$$

where $\lambda_p$ is the wavelength of the fluorescent peak and $\Delta\nu$ is the frequency full width at half maximum. The values of radiative transition rates $A$, the fluorescence branching ratios $\beta$, the radiative lifetime $\tau_r$ and stimulated emission cross-section $\sigma_p$ of the $^4F_{3/2} \rightarrow {}^4I_J$ transition are presented in Table 2. In general, people are interested in the transition $^4F_{3/2} \rightarrow {}^4I_{11/2}$ of the $Nd^{3+}$ ion for its use in the laser systems. The emission cross-section $\sigma_p$ of $^4F_{3/2} \rightarrow {}^4I_{11/2}$ transition of $Nd^{3+}$ ion is one of the most important parameters for laser design. In this work, the stimulated emission cross-section of $^4F_{3/2} \rightarrow {}^4I_{11/2}$ fluorescence transition of $Nd^{3+}$ ion is $1.16 \times 10^{-20}$ cm$^2$, which is comparable with those shown by glasses used in solid state laser applications [56].

## 4. Conclusions

The NIR-luminescent xerogels covalently bonded with ternary lanthanide (Ln = Er, Nd, Yb) complex were prepared via in situ synthesis method. No cracks were observed in the obtained xerogel-bonded Ln complexes, and these xerogel materials appear homogeneous as shown by SEM images. The NIR-luminescent properties of these materials show that the ligands shield the lanthanide ions well from their surroundings and efficiently transfer energy from their triplet states to the lanthanide ions. No quenching effects were detected with increasing the concentration of Ln ion from $N = 1/27$ to 1/11. The wide FWHM (76 nm) for the xerogel-bonded Er complex enables a wide gain bandwidth for the optical amplification. The Judd–Ofelt model has been applied to study the radiative spectral properties of xerogel-bonded Nd complex(1/11). The interactions between the lanthanide complex and the sil-

ica matrix, however, need to be fundamentally investigated further.

## Acknowledgements

The authors are grateful to the financial aid from the National Natural Science Foundation of China (Grant Nos. 20372060, 20340420326, 20490210, 206301040 and 20602035) and the MOST of China ("973" Program, Grant No. 2006CB601103). We are also grateful to Dr. E. Ma and Prof. J.G. Mao of the Fujian Institute of Research on the Structure of Matter, Chinese Academy of Sciences for assistance with the fluorescence measurements. We also thank Prof. C. Wang and Dr. Z.L. Chai (Changchun Institute of Applied Chemistry) for the SEM measurements.

## References

[1] J. Zhang, P.D. Badger, S.J. Geib, S. Petoud, Angew. Chem. Int. Ed. 44 (2005) 2508.
[2] M.H.V. Werts, R.H. Woudenberg, P.G. Emmerink, R. van Gassel, J.W. Hofstraat, J.W. Verhoeven, Angew. Chem. Int. Ed. 39 (2000) 4542.
[3] R.G. Sun, Y.Z. Wang, Q.B. Zheng, H.J. Zhang, A.J. Epstein, J. Appl. Phys. 87 (2000) 7589.
[4] P.G. Kik, M.L. Brongersma, A. Polman, Appl. Phys. Lett. 76 (2000) 2325.
[5] Q. Wang, N.K. Dutta, R. Ahrens, J. Appl. Phys. 95 (2004) 4025.
[6] M. Ryo, Y. Wada, T. Okubo, Y. Hasegawa, S. Yanagida, J. Phys. Chem. B 107 (2003) 11302.
[7] F. Vögtle, M. Gorka, V. Vicinelli, P. Ceroni, M. Maestri, V. Balzani, Chem. Phys. Chem. 2 (2001) 769.
[8] Y. Hasegawa, T. Ohkubo, K. Sogabe, Y. Kawamura, Y. Wada, N. Nakashima, S. Yanagida, Angew. Chem. Int. Ed. 39 (2000) 357.
[9] A.C. Franville, D. Zambon, R. Mahiou, Chem. Mater. 12 (2000) 428.
[10] C. Sanchez, G.J.A.A. Soler-Illia, F. Ribot, T. Lalot, C.R. Mayer, V. Cabuil, Chem. Mater. 13 (2001) 3061.
[11] R.J.P. Corriu, F. Embert, Y. Guari, A. Mehdi, C. Reyé, Chem. Commun. (2001) 1116.
[12] H.H. Li, S. Inoue, K. Machida, G. Adachi, Chem. Mater. 11 (1999) 3171.
[13] G.D. Qian, Z. Yang, M.Q. Wang, J. Lumin. 96 (2002) 211.
[14] G.D. Qian, M.Q. Wang, Mater. Res. Bull. 36 (2001) 2289.
[15] G.D. Qian, M.Q. Wang, Z. Yang, J. Phys. Chem. Solids 63 (2002) 1829.
[16] L.N. Sun, H.J. Zhang, L.S. Fu, F.Y. Liu, Q.G. Meng, C.Y. Peng, J.B. Yu, Adv. Funct. Mater. 15 (2005) 1041.
[17] F.Y. Liu, L.S. Fu, J. Wang, Q.G. Meng, H.R. Li, J.F. Guo, H.J. Zhang, New J. Chem. 27 (2003) 233.
[18] F.Y. Liu, L.S. Fu, J. Wang, Z. Liu, H.R. Li, H.J. Zhang, Thin Solid Films 419 (2002) 178.
[19] D.W. Dong, S.C. Jiang, Y.F. Men, X.L. Ji, B.Z. Jiang, Adv. Mater. 12 (2000) 646.
[20] Q.M. Wang, B. Yan, J. Mater. Chem. 14 (2004) 2450.
[21] H.R. Li, J. Lin, H.J. Zhang, H.C. Li, L.S. Fu, Q.G. Meng, Chem. Commun. (2001) 1212.
[22] H.R. Li, J. Lin, H.J. Zhang, L.S. Fu, Q.G. Meng, S.B. Wang, Chem. Mater. 14 (2002) 3651.
[23] K. Binnemans, P. Lenaerts, K. Driesen, C. Görller-Walrand, J. Mater. Chem. 14 (2004) 191.
[24] P. Lenaerts, E. Ryckebosch, K. Driesen, R. Van Deun, P. Nockemann, C. Görller-Walrand, K. Binnemans, J. Lumin. 114 (2005) 77.
[25] J.-P. Lecomte, A.K.D. Mesmaeker, M. Demeunynck, J. Lhomme, J. Chem. Soc., Faraday Trans. 89 (1993) 3261.
[26] Y.J. Cui, G.D. Qian, J.K. Gao, L.J. Chen, Z.Y. Wang, M.Q. Wang, J. Phys. Chem. B 109 (2005) 23295.
[27] D.W. Dong, B.Z. Jiang, Mater. Chem. Phys. 78 (2002) 501.
[28] S. Gago, J.A. Fernandes, J.P. Rainho, R.A. Sá Ferreira, M. Pillinger, A.A. Valente, T.M. Santos, L.D. Carlos, P.J.A. Ribeiro-Claro, I.S. Gonçalves, Chem. Mater. 17 (2005) 5077.
[29] R. Van Deun, P. Nockemann, C. Görller-Walrand, K. Binnemans, Chem. Phys. Lett. 397 (2004) 447.
[30] O.H. Park, S.Y. Seo, B.S. Bae, J.H. Shin, Appl. Phys. Lett. 82 (2003) 2787.
[31] M.P. Tsvirko, G.F. Stelmakh, V.E. Pyatosin, K.N. Solovyov, T.F. Kachura, Chem. Phys. Lett. 73 (1980) 80.
[32] M.P.O. Wolbers, F.C.J.M. van Veggel, B.H.M. Snellink-Ruël, J.W. Hofstraat, F.A.J. Geurts, D.N. Reinhoudt, J. Chem. Soc., Perkin Trans. 2 (1998) 2141.
[33] G. Boulon, A. Collombet, A. Brenier, M.T. Cohen-Adad, A. Yoshikawa, K. Lebbou, J.H. Lee, T. Fukuda, Adv. Funct. Mater. 11 (2001) 263.
[34] G.M. Davies, R.J. Aarons, G.R. Motson, J.C. Jeffery, H. Adams, S. Faulkner, M.D. Ward, Dalton Trans. (2004) 1136.
[35] B.R. Judd, Phys. Rev. 127 (1962) 750.
[36] G.S. Oflet, J. Chem. Phys. 37 (1962) 511.
[37] A.A. Kaminskii, E.L. Belokoneva, B.V. Mill, S.E. Sarkisov, K. Kurbanow, Phys. Status Solidi (a) 97 (1986) 279.
[38] T.S. Lomheim, L.G. DeShazer, J. Appl. Phys. 49 (1978) 5517.
[39] H.D. Jiang, J.Y. Wang, H.J. Zhang, X.B. Hu, H. Liu, J. Appl. Phys. 92 (2002) 3647.
[40] G.F. Wang, W.Z. Chen, Z.B. Li, Z.S. Hu, Phys. Rev. B 60 (1999) 15469.
[41] Y. Hasegawa, M. Yamamuro, Y. Wada, N. Kanehisa, Y. Kai, S. Yanagida, J. Phys. Chem. A 107 (2003) 1697.
[42] O.L. Malta, M.A. Couto dos Santos, L.C. Thompson, N.K. Ito, J. Lumin. 69 (1996) 77.
[43] P.C.R. Soares-Santos, H.I.S. Nogueira, V. Félix, M.G.B. Drew, R.A. Sá Ferreira, L.D. Carlos, T. Trindade, Chem. Mater. 15 (2003) 100.
[44] D.K. Sardar, J.B. Gruber, B. Zandi, J.A. Hutchinson, C.W. Trussell, J. Appl. Phys. 93 (2003) 2041.
[45] C. Koeppen, S. Yamada, G. Jiang, A.F. Garito, J. Opt. Am. Soc. B 14 (1997) 155.
[46] W.T. Carnall, P.R. Fields, K. Rajnak, J. Chem. Phys. 49 (1968) 4424.
[47] V. Mehta, G. Aka, A.L. Dawar, A. Mansingh, Opt. Mater. 12 (1999) 53.
[48] K. Driesen, S. Fourier, C. Görller-Walrand, K. Binnemans, Phys. Chem. Chem. Phys. 5 (2003) 198.
[49] B.R. Judd, J. Chem. Phys. 70 (1979) 4830.
[50] L.N. Sun, H.J. Zhang, Q.G. Meng, F.Y. Liu, L.S. Fu, C.Y. Peng, J.B. Yu, G.L. Zheng, S.B. Wang, J. Phys. Chem. B 109 (2005) 6174.
[51] C.K. Jørgensen, R. Reisfeld, J. Less-Common Met. 93 (1983) 107.
[52] A.A. Kaminskii, G. Boulon, M. Buoncristiani, B. Di Bartolo, A. Kornienko, V. Mironov, Phys. Status Solidi (a) 141 (1994) 471.
[53] M.H.V. Werts, R.T.F. Jukes, J.W. Verhoeven, Phys. Chem. Chem. Phys. 4 (2002) 1542.
[54] G.A. Kumar, A. Martinez, E.D.L. Rosa, J. Lumin. 99 (2002) 141.
[55] B. Chen, N. Dong, Q.J. Zhang, M. Yin, J. Xu, H. Liang, H. Zhao, J. Non-Cryst. Solids 341 (2004) 53.
[56] D.C. Brown, in D.L. MacAdam (Eds.), High-Peak-Power Nd: Glass Laser Systems, Springer Series in Optical Sciences, Berlin, Springer, 1981, Vol. 25.